Microfluid Nanofluid (2011) 10:107–122
DOI 10.1007/s10404-010-0651-y

RESEARCH PAPER

Effect of the skimming layer on electro-osmotic—Poiseuille flows of viscoelastic fluids

J. J. Sousa · A. M. Afonso · F. T. Pinho · M. A. Alves

Received: 16 January 2010 / Accepted: 26 May 2010 / Published online: 30 June 2010

Abstract An analytical solution is derived for the microchannel flow of viscoelastic fluids by combined electro-osmosis and pressure gradient forcing. The viscoelastic fluid is described by the Phan-Thien–Tanner model with due account for the near-wall layer depleted of macromolecules. This skimming layer is wider than the electric double layer (EDL) and leads to an enhanced flow rate relative to that of the corresponding uniform concentration flow case. The derived solution allows a detailed investigation of the flow characteristics due to the combined effects of fluid rheology, forcing strengths ratio, skimming layer thickness and relative rheology of the two fluids. In particular, when the EDL is much thinner than the skimming layer and simultaneously the viscosity of the Newtonian fluid inside this layer is much lower than that of the fluid outside, the flow is dominated by the characteristics of the Newtonian fluid. Outside these conditions, proper account of the various fluid layers and their properties must be considered for an accurate prediction of the flow characteristics. The analytical solution remains valid for the flow driven by a pressure gradient and its streaming potential, which is determined in the appendix.

Keywords Electro-kinetic effects · Phan-Thien–Tanner fluid · Skimming layer · Channel flow · Electro-osmosis Poiseuille flow

List of Symbols

a_1, a_2 and a_3	Coefficients of cubic equation
A_{chan}	Cross-section area of the channel (m^2)
$\bar{A}$, $\bar{B}$, $\bar{C}$, $\bar{D}$, $\bar{E}$ and $\bar{F}$	Functions to compact equations
De	Deborah number
e	Electron charge (1.6022×10^{-19} C)
E_x	x component of the electric gradient (V m^{-1})
$E_{x,\text{sp}}$	Streaming potential axial gradient (V m^{-1})
$f(\tau_{kk})$	PTT stress coefficient function
H	Microchannel half-height (m)
I'_{c}	Conduction current per unit width (A m^{-1})
I'_{s}	Streaming current per unit width (A m^{-1})
I'	Net electrical current per unit width (A m^{-1})
k_{B}	Boltzmann constant (1.3807×10^{-23} J K^{-1})
l	Microchannel length (m)
n_{o}	Ionic number concentration (m^{-3})
p	Pressure (Pa)

J. J. Sousa
Lactogal, Direcção Engenharia Industrial, Rua Campo Alegre 830, 4150-171 Porto, Portugal
e-mail: jeremias.sousa@lactogal.pt
URL: http://www.lactogal.pt

A. M. Afonso · M. A. Alves
Departamento de Engenharia Química, CEFT, Faculdade de Engenharia da Universidade do Porto, Rua Dr. Roberto Frias s/n, 4200-465 Porto, Portugal
e-mail: aafonso@fe.up.pt

M. A. Alves
e-mail: mmalves@fe.up.pt

F. T. Pinho (✉)
Departamento de Engenharia Mecânica, CEFT, Faculdade de Engenharia da Universidade do Porto, Rua Dr. Roberto Frias s/n, 4200-465 Porto, Portugal
e-mail: fpinho@fe.up.pt

$p_{,x}$	Axial pressure gradient (Pa m^{-1})
P_{sur}	Wetted perimeter of the channel (m)
Q	Volumetric flow rate per unit width (m^2 s^{-1})
t	Time (s)
T	Absolute temperature (K)
U_N	Newtonian bulk velocity (m s^{-1})
u_{sh}	Helmholtz–Smoluchowski velocity based on the polymer viscosity coefficient (m s^{-1})
u_{sh}^s	Helmholtz–Smoluchowski velocity based on the solvent viscosity coefficient (m s^{-1})
x	Axial coordinate (m)
y	Transverse coordinate (m)
z	Valence of ions

Tensors and Vectors

D	Rate of deformation tensor (s^{-1})
E	External applied electric field (V m^{-1})
I	Unitary tensor
u	Velocity vector (m s^{-1})
$\boldsymbol{\tau}$	Extra-stress tensor (Pa)

Greek symbols

β	Ratio of viscosity coefficients
δ_L	Thickness of the layer depleted of macro-molecules (skimming layer) (m)
ε	PTT parameter
$\in$	Dielectric constant of the fluid (C V^{-1} m^{-1})
ϕ	Electric potential (V)
$\dot{\gamma}$	Shear rate (s^{-1})
Γ	Ratio of pressure to electro-osmotic driving forces
η	Polymer viscosity coefficient (PTT model) (Pa s)
η_s	Viscosity of Newtonian fluid in the skimming layer (Pa s)
κ^2	Debye–Hückel parameter (m^{-2})
λ	Relaxation time of polymeric fluid (s)
μ	Viscometric viscosity (Pa s)
ρ_e	Electric charge density (C m^{-3})
σ_t	Total electric conductivity (Ω^{-1} m^{-1})
σ_{fluid}	Fluid bulk conductivity (Ω^{-1} m^{-1})
σ_{sur}	Wall surface conductivity (Ω^{-1})
τ_{xx}, τ_{yy}	Normal stresses (Pa)
τ_{xy}	Shear stress (Pa)
τ_{kk}	Trace of the extra-stress tensor (Pa)
ξ	EDL thickness (m)
ψ	Potential field (V)
ψ_0	Wall zeta potential (V)
Ψ_1	First normal stress difference coefficient
Υ_1	Dimensionless number

Mathematical

∇	Upper-convected derivative

Subscripts

E	Related to electro-osmotic flow
EP	Related to pressure-driven and electro-osmotic combined effects
I	Refers to skimming layer (fluid layer I)
II	Refers to bulk flow (fluid layer II)
N	Refers to Newtonian fluid
P	Related to pressure-driven flow
sh	Refers to Helmholtz–Smoluchowski
sp	Refers to streaming potential
x	Refers to the axial coordinate
κ	Refers to Debye–Hückel parameter

Superscript

_ (overbar)	Dimensionless quantity

1 Introduction

The advent of cheap micro-fabrication techniques is promoting the widespread adoption of microfluidic flow devices by a large number of industrial applications, especially those dealing with bio-fluids, but also including new energy systems, such as fuel cell systems where there is flow through porous media and membranes. Accurate flow control in these devices requires techniques that can easily be miniaturized and an obvious candidate is electricity-related forcing taking advantage of electro-kinetic phenomena. An overview of electro-kinetic techniques can be found in Bruus (2008).

When a polar fluid is brought in contact with a solid surface chemical equilibrium leads to a spontaneous charge being acquired by the wall and this in turn forces the formation of a near-wall layer of mobile ions containing a higher concentration of counter-ions as the co-ions moved away from the wall. This is the diffuse layer and closer to the wall there is a very thin layer of immobile ions forming the Stern layer. Together they form the electric double layer (EDL) and electro-osmosis flow is obtained when an external electric field is applied between the inlet and outlet due to the Coulomb forces acting on the EDL ions. In addition it is possible to induce flow by pressure gradient, but electro-kinetic effects in micro-channels can also create spontaneous electro-osmosis in Poiseuille flows, i.e. in the absence of an imposed electric field a Poiseuille flow advects counter-ions to the channel outlet thus creating an adverse streamwise electric potential, or streaming potential (Vainshtein and Gutfinger 2002), leading to electro-osmotic flow in the opposite direction. More details on electro-kinetic effects and in particular on electro-osmosis

can be found in Probstein (2003) and Bruus (2008), amongst others.

The principle of electro-osmosis was demonstrated by Reuss (1809) early in the nineteenth century and has been subsequently developed, especially over the last 30 years. Today, there are rigorous models of electro-osmotic flows in microchannels for Newtonian fluids, such as those of Burgreen and Nakache (1964) and Dutta and Beskok (2001) for weak and strong surface potentials, respectively. Synthetic and bio-fluids are often made from complex molecules that impart non-linear rheological behaviour, called non-Newtonian to distinguish from the common linear stress rate-of-strain behaviour of fluids made from small molecules. The first treatments of non-Newtonian effects, by Das and Chakraborty (2006) and Chakraborty (2007) amongst others, were limited to inelastic power law fluids, and this same model was used by Zhao et al. (2008) in their investigation of steady electro-osmosis flow in a slit microchannel under the Debye–Hückel approximation. They found an analytical solution only for three discrete values of the power law index (n) and proceeded to obtain and validate an approximate solution for any value of n.

The extension to viscoelastic fluids was done almost simultaneously by Park and Lee (2008a, b). Park and Lee (2008a) derived a semi-analytical expression for the Helmholtz–Smoluchowski velocity under pure electro-osmosis conditions for the full Phan-Thien–Tanner (PTT) constitutive equation. The profile of streamwise velocity involves the numerical integration of the transverse velocity gradient, which is given by the real solution of a cubic equation. Park and Lee (2008b) used a finite volume method to calculate numerically the flow of the full PTT model in a rectangular duct under the action of electro-osmosis and a pressure gradient. For the simplified PTT model, which has a zero second normal stress difference, there is an analytical solution for the combined electro-osmosis-Poiseuille flow in a two-dimensional channel, which was obtained by Afonso et al. (2009) under the Debye–Hückel approximation. This work is a follow-up dealing with the viscoelastic flow in the presence of a depleted region of macromolecules near the walls.

In solutions of macromolecules there are additional effects that need to be accounted for in electro-osmosis due to the more complex interactive forces between the wall and the macromolecules and the obvious blockage that the wall imposes on molecular motion. As a consequence there can be wall adsorption or depletion as explained by Olivares et al. (2009), the latter being more common. Their measurements of the electroosmotic mobility of carboxymethyl cellulose solutions (CMC) in a straight channel revealed that the fluid was not homogeneous across the channel and the data are consistent with the existence of a near-wall layer containing a lower concentration of polymer. In addition, Olivares et al. (2009) present a simple model, where the fluids in the bulk and in the depleted layer are described by the inelastic Generalized Newtonian constitutive equation with a power law for the viscosity function. The electro-osmotic flow of inelastic Generalized Newtonian fluids with a Newtonian skimming layer had been previously studied from a theoretical point of view by Berli and Olivares (2008), including the power law model, but usually the polymer solutions have viscoelastic characteristics and their rheology are described by viscoelastic constitutive equations that contain memory effects in addition to a variable viscosity, which is not as simple as a power law, but contains a Newtonian plateau at low shear rates. In this work, we exactly address this problem by analysing the flow of non-Newtonian fluids described by the viscoelastic PTT constitutive equation (PTT model) in the presence of a near-wall region depleted of macromolecules. Thus, this is an extension of our previous work for homogeneous viscoelastic fluids (Afonso et al. 2009) to deal with this wall phenomenon. Even though the skimming layer is thicker than the Debye layer, in our analysis we keep generality by allowing the electrostatic field to act upon both the depleted layer and the bulk flow, in contrast to Berli and Olivares (2008) and Olivares et al. (2009), who always considered the bulk flow to be electrically neutral.

In this article, an analytical solution is derived for the micro-channel flow of viscoelastic fluids by combined electro-osmosis and pressure gradient forcing under fully developed conditions. The viscoelastic fluid is described by the PTT model (Phan-Thien and Tanner 1977) with due account for the near-wall layer depleted of macromolecules and behaving as a Newtonian fluid. This skimming layer is wider than the EDL and leads to an enhanced flow rate relative to that of the corresponding uniform concentration flow case. The derived solution allows a detailed investigation of the flow characteristics due to the combined effects of fluid rheology, forcing strengths ratio and the ratio between the thicknesses of the skimming layer and of the EDL.

Section 2 presents the governing equations and boundary conditions and is followed in Sect. 3 by the analytical solution. Explicit expressions are provided for the velocity profile, shear and normal stresses in dimensional and nondimensional forms as well as for the nondimensional viscosity, first normal stress difference coefficient and flow rate. The results are discussed in Sect. 4, with the main conclusions summarised in Sect. 5.

Sometimes the electrical field E_x is not applied externally, but is a consequence of the motion of the ions in the flow induced by the applied pressure gradient. This movement of ions is an electrical current known as the streaming current. The accumulation of counter-ions at the end of a channel sets up an electric field, $E_{x\text{-sp}}$, associated

with its streaming potential, ϕ_{sp}, and this electric field itself creates a current. In equilibrium there will be a net zero charge current so for a specific imposed pressure gradient there will be a well-defined streaming potential electrical field. The characteristics of this combined flow are given by the general flow solution once $E_{x\text{-sp}}$ is known for a specific pressure gradient. This explicit relation between the imposed pressure gradient and the streaming potential is analytically derived and presented in the Appendix.

2 Governing equations

Figure 1 shows schematically the flow geometry and illustrates also the electro-osmosis phenomenon showing in addition the depletion layer, also called skimming layer, since it is here assumed that there are repulsive forces between the macromolecules and the wall. The nomenclature used is that of our previous work (Afonso et al. 2009). Close to the wall there is a Newtonian fluid and in the core there is the viscoelastic fluid. Both layers are subject to the electro-kinetic field and the pressure gradient forcings, but as we shall see the direct impact of electro-osmosis on the PTT velocity profile is fairly weak. The layer depleted of macromolecules has a thickness (δ_L) and it is usually larger than the thickness (ξ) of the EDL. This is so because the thickness of the skimming layer is of the order of the radius of gyration of the macromolecules, whereas the EDL is often of the order of 10 to about 100 nm, i.e. $\xi < \delta_L$ (Olivares et al. 2009). Given this flow structure electro-osmosis is usually present essentially inside the skimming layer and the electrokinetic effects are carried into the outer viscoelastic fluid region by viscous dragging at the interface. However, for generality the analytical solution derived here takes into account electro-kinetic effects also within the viscoelastic fluid. If macromolecular depletion in the skimming layer is complete, the fluid there is the Newtonian solvent.

Regardless of whether there is a skimming layer the EDL is composed of a very thin layer of stagnant fluid densely populated with counter-ions, called the Stern layer, followed by a mobile layer of counter-ions at a smaller concentration, denoted diffuse layer (Lyklema et al. 1998). The total charge in the system is neutral, i.e. there are as many ions at the wall as counter-ions at the EDL.

As a consequence of the described fluid model, the flow governing equations to be solved for fully developed flow are the continuity Eq. 1 and the following modified form of the Cauchy Eq. 2.

$$\nabla \cdot \mathbf{u} = 0 \tag{1}$$

$$-\nabla p + \nabla \cdot \boldsymbol{\tau} + \rho_e \mathbf{E} = \mathbf{0} \tag{2}$$

where $\mathbf{u}$ is the velocity vector, p is the pressure, and $\boldsymbol{\tau}$ is the fluid extra-stress tensor. In the skimming layer this extra-stress tensor describes a Newtonian fluid of viscosity η_s via Eq. 3, whereas elsewhere the fluid is described by the PTT model of Eq. 4. The $\rho_e\mathbf{E}$ term represents the applied external electric field (or the induced streaming potential in Poiseuille flow with electroviscous effects), where ρ_e is the net electric charge density in the fluid. If the EDL is much thinner than the skimming layer the electrical field forcing ($\rho_e\mathbf{E}$) is negligible outside the skimming layer, but for generality we keep the electro-osmotic forcing inside and outside the skimming layer and we consider always that the EDL is thinner, but not necessarily much thinner, than the skimming layer. The electric field $\mathbf{E}$ is related to the existing potential via $\mathbf{E} = -\nabla\Phi$, with $\Phi = \psi + \phi$, where ϕ is the applied streamwise potential and ψ is the potential spontaneously formed by the interaction between the walls and the fluid, which only varies in the cross-stream direction. We also consider that the electric properties of the polymer solution and Newtonian solvent are identical. As described, the rheological models for the fluid inside and outside the skimming layer are expressed mathematically as

– for the solvent (layer I):

$$\boldsymbol{\tau} = 2\eta_s \mathbf{D} \tag{3}$$

– for the polymeric liquid (layer II):

$$f(\mathrm{tr}\boldsymbol{\tau})\boldsymbol{\tau} + \lambda \overset{\nabla}{\boldsymbol{\tau}} = 2\eta \mathbf{D}, \tag{4}$$

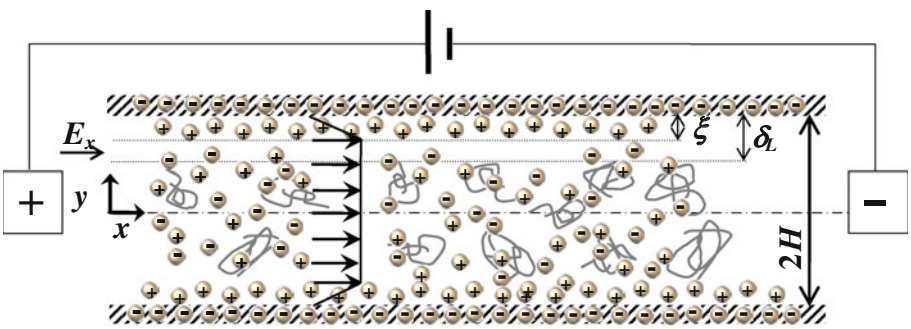

Fig. 1 Schematic representation of the electro-osmotic flow in a microchannel with a skimming layer

where the rate of deformation tensor is $\mathbf{D} = (\nabla\mathbf{u} + (\nabla\mathbf{u})^{\mathrm{T}})/2$, λ is the relaxation time of the polymeric fluid having a viscosity coefficient η, and $\overset{\nabla}{\boldsymbol{\tau}}$ denotes the upper-convected Oldroyd derivative defined as:

$$\overset{\nabla}{\boldsymbol{\tau}} = \frac{D\boldsymbol{\tau}}{Dt} - (\nabla\mathbf{u})^{\mathrm{T}}\cdot\boldsymbol{\tau} - \boldsymbol{\tau}\cdot\nabla\mathbf{u} \tag{5}$$

The stress coefficient for the PTT model is given by its linear form (Phan-Thien and Tanner 1977), $f(\mathrm{tr}\boldsymbol{\tau}) = 1 + (\varepsilon\lambda/\eta)\mathrm{tr}\boldsymbol{\tau}$, introducing the extensibility parameter ε, which is responsible for bounding the extensional viscosity of the model. The extensional viscosity is relevant whenever there are regions of extension flow, but the stress function gives the model its nonlinear nature, which impacts on all other fluid properties.

Although the PTT model was derived by Phan-Thien and Tanner (1977) from considerations of network theories for polymer melts, it can also be applied to polymer solutions provided its rheology matches that of the fluid. This viscoelastic constitutive equation obeys all principles of invariance and objectivity of continuum mechanics related to viscoelastic materials (Astarita and Marrucci 1974). In its original form it contains an extra parameter (χ) that quantifies the slip velocity between the molecular network and the continuum medium, which is responsible for a non-zero second normal stress difference, but here a simpler version with $\chi = 0$ is used, so exhibiting a zero second normal stress difference coefficient.

In pure shear flow the shear viscosity (μ) of the PTT model is given by

$$\mu = \sqrt[3]{-\frac{b}{2} + \sqrt{\frac{b^2}{4} + \frac{a^3}{27}}} + \sqrt[3]{-\frac{b}{2} - \sqrt{\frac{b^2}{4} + \frac{a^3}{27}}} \tag{6}$$

with $a = \eta^2/(2\varepsilon\lambda^2\dot{\gamma}^2)$ and $b = -\eta^3/(2\varepsilon\lambda^2\dot{\gamma}^2)$. The shear rate $\dot{\gamma}$ is related to the second invariant of the rate of deformation tensor and given by $\dot{\gamma} = \sqrt{2\mathrm{tr}\mathbf{D}^2}$. This viscosity is plotted in Fig. 2 in normalised form for some characteristic values of the parameters. At low shear rates there is a Newtonian plateau of constant viscosity equal to η followed by a shear-thinning behaviour at higher shear rates, as is typical of non-Newtonian fluids with no yield stress. The transition between the Newtonian plateau and the variable viscosity region takes place at $\dot{\gamma} \approx 1/\lambda$, consequently the plot of μ/η versus $\lambda\dot{\gamma}$ is independent of λ. The PTT model also exhibits a shear thinning first normal stress difference coefficient in pure shear flow, a characteristic property of viscoelastic fluids, but of no consequence for the present solution. The corresponding equation can be found in Alves et al. (2001).

The flow under analysis is steady, fully developed and the electric double layers forming near each wall are sufficiently thin to be considered independent of each other. In addition, the flow geometry and conditions are symmetric, so only half the channel needs to be considered. These

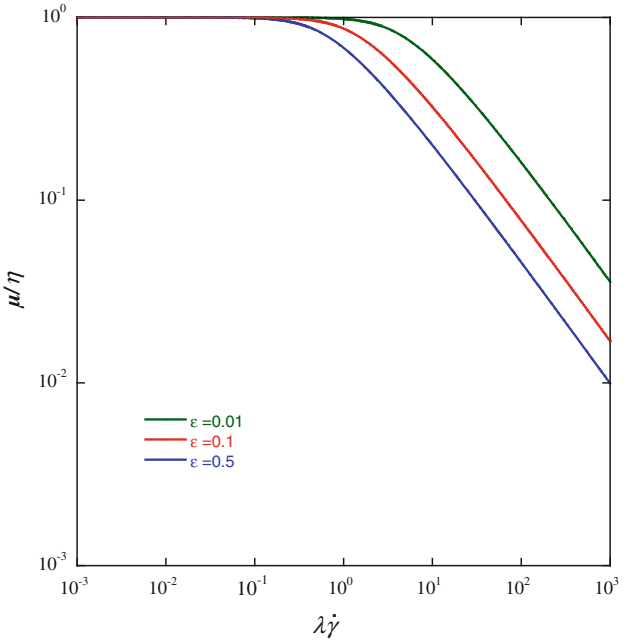

Fig. 2 Variation of the normalised shear viscosity with normalised shear rate for a PTT fluid

EDL (or Debye layers) are formed spontaneously from the contact between the dielectric walls and the polar fluid as schematically shown in Fig. 1. These conditions imply that the Nernst–Planck equations governing the ionic and induced electric potential field (ψ) distributions simplify so that in the EDL ψ is expressed by the following Poisson equation (Park et al. 2007):

$$\nabla^2\psi = -\frac{\rho_{\mathrm{e}}}{\in} \tag{7}$$

where $\in$ is the dielectric constant of the solution assumed constant. Following Bruus (2008) the electric charge density distribution in equilibrium near a charged surface, as in this fully developed flow geometry, is given by

$$\rho_{\mathrm{e}} = -2n_0 ez\sinh\left(\frac{ez}{k_{\mathrm{B}}T}\psi\right) \tag{8}$$

with n_0 representing the ionic density, e is the elementary electronic charge, z is the valence of the ions, k_{B} is the Boltzmann constant and T is the absolute temperature. Back-substituting Eq. 8 into Eq. 7 leads to the Poisson–Boltzmann equation, the integration of which provides the distribution of ψ.

2.1 Boundary conditions

As mentioned above, only half of the channel is considered ($0 \le y \le H$) given the flow symmetry, with H denoting the half-channel width. At the wall the no-slip condition applies, here for an immobile wall, and at the centreplane

flow symmetry conditions apply (flow symmetry conditions are anti-symmetry of the shear stress, hence $\tau_{xy} = 0$ at $y = 0$). At the interface between the skimming layer and the bulk of the fluid a no-slip condition for velocity is valid, i.e. both fluids move at the same velocity at their interface.

Regarding the Poisson–Boltzmann equation governing the electric charge distribution, at the interface between the dielectric wall and the electrolyte fluid there is a wall potential ψ_0, also called the zeta potential, which depends on the properties of the wall and fluid. The constant potential gradient of the applied electric field in the streamwise direction ($\Delta\phi/l$, where l is the channel length) is sufficiently weak not to interfere with the induced ion distribution across the channel, i.e., $\Delta\phi/l \ll \psi_0/\xi$. These are the conditions of the so-called standard electro-kinetic model (see Hunter (2001) or Probstein (2003) for further details). The potential ψ decreases very quickly with distance from the wall and even though it is not null at the skimming layer interface, it is sufficiently small to have a negligible direct influence upon the viscoelastic fluid lying outside the skimming layer, as will be seen later.

For small zeta potentials the EDL thickness is thin and for small values of $ez\psi/(k_BT)$, Eq. (8) can be linearized, i.e., $\sinh x \approx x$. This is called the Debye–Hückel approximation, which we invoke here, thus limiting the zeta potential to values smaller than 26 mV at room temperatures (Burgreen and Nakache (1964), Dutta and Beskok (2001)).

3 Analytical solution

We start by integrating the Poisson–Boltzmann equation considering the Debye–Hückel hypothesis of Sect. 2.1:

$$\frac{d^2\psi}{dy^2} = \frac{2n_0 ez \sinh\left(\frac{ez}{k_BT}\psi\right)}{\in} \rightarrow \frac{d^2\psi}{dy^2} = \frac{2n_0 e^2 z^2 \psi}{k_BT \in} \tag{9}$$

Defining the Debye–Hückel parameter (κ) as $\kappa^2 = 2n_0e^2z^2/(k_BT \in)$, which is related to the EDL thickness by $\xi = 1/\kappa$, the integration of Eq. 9 leads to the following transverse distribution of the electric potential

$$\psi = \psi_0 \frac{\cosh(\kappa y)}{\cosh(\kappa H)} \tag{10}$$

where ψ_0 is the wall potential, also known as zeta potential.

The corresponding distribution of the electric charge density is obtained by back substitution in Eq. 8 and is given by $\rho_e = -\in \kappa^2 \psi_0 (\cosh(\kappa y)/\cosh(\kappa H))$, which is positive when the wall charge is negative, as it should.

We can now integrate the momentum equation, which for the streamwise component is expressed as

$$\frac{d\tau_{xy}}{dy} = -\rho_e E_x + p_{,x} \rightarrow \frac{d\tau_{xy}}{dy} = \in \psi_0 E_x \kappa^2 \frac{\cosh(\kappa y)}{\cosh(\kappa H)} + p_{,x} \tag{11}$$

and its integration results in the following shear stress distribution

$$\tau_{xy} = \in \psi_0 E_x \kappa \frac{\sinh(\kappa y)}{\cosh(\kappa H)} + p_{,x} y. \tag{12}$$

Note that the constant of integration appearing from the integration of Eq. 11 is null since $\tau_{xy} = 0$ at the centreplane.

To determine the velocity field, it is now necessary to consider the expressions for the shear stress from the corresponding rheological equations, a task performed in the next two subsections.

3.1 Skimming layer (layer I)

Inside the skimming layer ($H - \delta_L \le y \le H$) the fluid is Newtonian and the corresponding constitutive relation (Eq. 3) is used to determine the shear stress, which upon substitution onto Eq. 12 gives the following expression for the velocity gradient:

$$\eta_s \frac{du}{dy} = \in \psi_0 E_x \kappa \frac{\sinh(\kappa y)}{\cosh(\kappa H)} + p_{,x} y. \tag{13}$$

Integration of Eq. 13 subject to the no-slip boundary condition at the wall ($u = 0$ at $y = H$) gives the velocity profile

$$u_I(y) = u_{E-I}(y) + u_{P-I}(y) \tag{14a}$$

with

$$u_{E-I}(y) = \frac{-\in \psi_0 E_x}{\eta_s}\left[1 - \frac{\cosh(\kappa y)}{\cosh(\kappa H)}\right];$$
$$u_{P-I}(y) = \frac{-p_{,x}}{2\eta_s}\left(H^2 - y^2\right). \tag{14b}$$

This velocity profile is written as the sum of two contributions: u_E is the velocity profile for pure electro-osmotic flow (in the absence of pressure gradient forcing) and u_P is for pure Poiseuille flow (in the absence of electro-osmosis). The two contributions are independent since the superposition principle is valid for the Newtonian fluid (Afonso et al. 2009).

3.2 Outside the skimming layer (layer II)

Outside the skimming layer ($0 \le y \le H - \delta_L$) the PTT fluid leads to a more complex expression. As in other fully

developed channel flows of the PTT fluids (cf. Afonso et al. (2009), Oliveira and Pinho (1999)), simplification of Eqs. (4) and (5) leads to the following relationships between the velocity gradient and the two non-zero components of the extra-stress tensor:

$$\frac{\mathrm{d}u}{\mathrm{d}y} = \frac{1}{\eta}\left(1 + \frac{\varepsilon\lambda}{\eta}\tau_{xx}\right)\tau_{xy} \tag{15}$$

with

$$\tau_{xx} = \frac{2\lambda}{\eta}\tau_{xy}^2. \tag{16}$$

A consequence of Eqs. 12 and 16 is the transverse distribution of the normal stress for the PTT fluid given by

$$\tau_{xx} = \frac{2\lambda}{\eta}\left(\in \psi_0 E_x \kappa \frac{\sinh(\kappa y)}{\cosh(\kappa H)} + p_{,x} y\right)^2, \tag{17}$$

whereas inside the skimming layer the Newtonian solvent implies $\tau_{xx} = 0$ under fully developed flow conditions.

Back substitution of Eqs. 16 and 12 into Eq. 15 provides the differential equation (18) for the velocity gradient:

$$\frac{\mathrm{d}u}{\mathrm{d}y} = \frac{1}{\eta}\left\{1 + \frac{\varepsilon\lambda}{\eta}\left[\frac{2\lambda}{\eta}\left(\in \psi_0 E_x \kappa \frac{\sinh(\kappa y)}{\cosh(\kappa H)} + p_{,x} y\right)^2\right]\right\} \times \left(\in \psi_0 E_x \kappa \frac{\sinh(\kappa y)}{\cosh(\kappa H)} + p_{,x} y\right) \tag{18}$$

This equation can be integrated subject to the boundary condition of equal velocities at the interface between the skimming layer and the bulk flow, i.e. at $y = H - \delta_{\mathrm{L}}$, the velocity $u_{\mathrm{Newtonian}}(H - \delta_{\mathrm{L}}) = u_{\mathrm{PTT}}(H - \delta_L)$, leading to the velocity profile

$$u_{\mathrm{II}}(y) = u_{\mathrm{E-II}}(y) + u_{\mathrm{P-II}}(y) + u_{\mathrm{EP-II}}(y) \tag{19a}$$

with

$$u_{\mathrm{E-II}}(y) = \in \psi_0 E_x \left\{\frac{1}{\eta}[\bar{A} - \bar{E}] + \frac{1}{\eta_{\mathrm{s}}}[\bar{E} - 1]\right\} - 2\frac{\varepsilon\lambda^2}{\kappa}\left(\frac{\in \psi_0 E_x \kappa}{\eta}\right)^3 \left[\bar{C}(\bar{A} - \bar{E}) + \frac{\bar{E}^3 - \bar{A}^3}{3}\right] \tag{19b}$$

$$u_{\mathrm{P-II}}(y) = \frac{p_{,x}}{2}\left[\frac{y^2 - (H - \delta_{\mathrm{L}})^2}{\eta} + \frac{(H - \delta_{\mathrm{L}})^2 - H^2}{\eta_s}\right] + \frac{\varepsilon\lambda^2 p_{,x}^3}{2\eta^3}\left[y^4 - (H - \delta_{\mathrm{L}})^4\right] \tag{19c}$$

$$u_{\mathrm{EP-II}}(y) = \frac{6\varepsilon\lambda^2 p_{,x}}{\eta\kappa^2}\left(\frac{\in \psi_0 E_x \kappa}{\eta}\right) \times \left\{\frac{\in \psi_0 E_x \kappa}{\eta}\left[\frac{\kappa\bar{D}}{2}(y\bar{A}\bar{B} - (H - \delta_{\mathrm{L}})\bar{E}\bar{F}) - \frac{\bar{C}}{4}\left[(\kappa y)^2 - \kappa^2(H - \delta_{\mathrm{L}})^2\right] + \frac{(\bar{E}^2 - \bar{A}^2)}{4}\right] + \left[\frac{p_{,x}}{\eta\kappa}\left[\bar{A}\left[(\kappa y)^2 + 2\right] - \bar{E}\left[\kappa^2(H - \delta_{\mathrm{L}})^2 + 2\right] - 2\bar{D}[\kappa y\bar{B} - \kappa(H - \delta_{\mathrm{L}})\bar{F}]\right]\right]\right\}, \tag{19d}$$

where for compactness the following quantities are used: $\bar{A} = \cosh(\kappa y)/\cosh(\kappa H)$, $\bar{B} = \sinh(\kappa y)/\sinh(\kappa H)$, $\bar{C} = 1/\cosh^2(\kappa H)$, $\bar{D} = \tanh(\kappa H)$, $\bar{E} = \cosh[\kappa(H - \delta_{\mathrm{L}})]/\cosh(\kappa H)$ and $\bar{F} = \sinh[\kappa(H - \delta_{\mathrm{L}})]/\sinh(\kappa H)$.

The velocity profile outside the skimming layer has an extra contribution, in addition to the pure electro-osmotic and pure Poiseuille flow terms. The extra term ($u_{\mathrm{EP-II}}$) accounts simultaneously for both effects and is non-zero only when there is simultaneous forcing by pressure gradient and electric potential, thus showing that for the PTT fluid the superposition principle no longer applies (Afonso et al. 2009).

3.3 Nondimensional velocity profile

It is worth presenting the main equations in a normalised form. For this purpose the following quantities are introduced: $\bar{y} = y/H$ and $\bar{\kappa} = \kappa H$ are nondimensional lengths, the Helmholtz–Smoluchowski electro-osmotic velocity $u_{\mathrm{sh}} = -\in \psi_0 E_x/\eta$ is used to normalise the velocity and the Deborah number is based on the EDL thickness and u_{sh}, $De_k = \lambda u_{\mathrm{sh}}/\xi = \lambda\kappa u_{\mathrm{sh}}$ as in Afonso et al. (2009). See also this reference for other definitions of Deborah number used in the context of pure Poiseuille flows. The use of the polymer viscosity coefficient to define the Helmholtz–Smoluchowski velocity and for normalisation of the velocity profile is for consistency with the previous work and to consider the limiting case of a zero skimming layer thickness. Physically it is more logical to use the viscosity of the fluid in the skimming layer, the Newtonian solvent viscosity. The corresponding Helmholtz–Smoluchowski velocity is given as $u_{\mathrm{sh}}^{\mathrm{s}} = \beta u_{\mathrm{sh}}$, where β is the viscosity ratio defined below.

To account for the combined forcing of pressure gradient and electro-osmosis, the nondimensional ratio between these two forcings is given by $\Gamma = -(H^2/\in \psi_0)(p_{,x}/E_x)$. Finally, the presence of a Newtonian fluid in the skimming layer introduces the ratio of viscosity coefficients $\beta = \eta/\eta_{\mathrm{s}}$ and the normalized skimming layer thickness $\bar{\delta}_{\mathrm{L}} = \delta_{\mathrm{L}}/H$.

Inside the skimming layer the normalised velocity profile is rewritten as

$$\frac{u_{\mathrm{I}}(\bar{y})}{u_{\mathrm{sh}}} = (1-\bar{A})\beta - \frac{1}{2}\beta\Gamma\left(1-\bar{y}^2\right) \tag{20}$$

where the first and second terms on the right-hand-side (RHS) are the normalized $u_{\mathrm{E-I}}$ and $u_{\mathrm{P-I}}$ contributions. The normalised profile outside the skimming layer is written as

$$\frac{u_{\mathrm{II}}(\bar{y})}{u_{\mathrm{sh}}} = \bar{u}_{\mathrm{E-II}}(\bar{y}) + \bar{u}_{\mathrm{P-II}}(\bar{y}) + \bar{u}_{\mathrm{EP-II}}(\bar{y}) \tag{21a}$$

with

$$\bar{u}_{\mathrm{E-II}}(\bar{y}) = [\bar{E}-\bar{A}] + \beta[1-\bar{E}] + 2\varepsilon De_{\kappa}^2\left[\bar{C}(\bar{A}-\bar{E}) + \frac{\bar{E}^3-\bar{A}^3}{3}\right] \tag{21b}$$

$$\bar{u}_{\mathrm{P-II}}(\bar{y}) = \frac{\Gamma}{2}\left[\bar{y}^2 - \left(1-\bar{\delta}_{\mathrm{L}}\right)^2\right] \times \left\{1 + \frac{\varepsilon De_{\kappa}^2\Gamma^2}{\bar{\kappa}^2}\left[\bar{y}^2 + \left(1-\bar{\delta}_{\mathrm{L}}\right)^2\right]\right\} + \frac{\Gamma\beta}{2}\left[\left(1-\bar{\delta}_{\mathrm{L}}\right)^2 - 1\right] \tag{21c}$$

$$\bar{u}_{\mathrm{EP-II}}(\bar{y}) = \frac{6\varepsilon De_{\kappa}^2\Gamma}{\bar{\kappa}^2}\left\{\frac{\bar{D}}{2}\left[\bar{\kappa}\bar{y}\bar{A}\bar{B} - \bar{\kappa}\left(1-\bar{\delta}_{\mathrm{L}}\right)\bar{E}\bar{F}\right] - \frac{\bar{C}}{4}\left[(\bar{\kappa}\bar{y})^2 - \bar{\kappa}^2\left(1-\bar{\delta}_{\mathrm{L}}\right)^2\right] + \frac{(\bar{E}^2-\bar{A}^2)}{4} - \frac{\Gamma}{\bar{\kappa}^2}\left[\bar{A}\left[(\bar{\kappa}\bar{y})^2+2\right] - \bar{E}\left[\bar{\kappa}^2\left(1-\bar{\delta}_{\mathrm{L}}\right)^2+2\right] - 2\bar{D}\left[\bar{\kappa}\bar{y}\bar{B} - \bar{\kappa}\left(1-\bar{\delta}_{\mathrm{L}}\right)\bar{F}\right]\right]\right\} \tag{21d}$$

The alternative velocity solution normalised by the Helmholtz–Smoluchowski velocity based on the solvent viscosity is simply obtained as

$$\frac{u}{u_{\mathrm{sh}}^{\mathrm{s}}} = \frac{u}{u_{\mathrm{sh}}}\frac{1}{\beta} = \frac{\bar{u}}{\beta} \tag{22}$$

bearing in mind that De_{κ} is still defined with u_{sh}. Equation 22 will be used occasionally in the results section to improve our understanding of the results.

3.4 Viscosity and stresses

From the velocity profiles and its derivatives, one can determine the profiles of shear viscosity (μ) and of the first normal stress difference coefficient (Ψ_1)

$$\text{Layer I:} \frac{\mu}{\eta} = \frac{1}{\beta} \quad \text{and} \quad \frac{\Psi_1}{2\lambda\eta} = 0 \tag{23a}$$

$$\text{Layer II:} \frac{\mu}{\eta} = \frac{1}{1 + 2\varepsilon De_{\kappa}^2\left[\Gamma\bar{y}/\bar{\kappa} - \bar{B}\bar{D}\right]^2} \quad \text{and} \quad \frac{\Psi_1}{2\lambda\eta} = \frac{\bar{\kappa}^4}{\left[\bar{\kappa}^2 + 2\varepsilon De_{\kappa}^2(\bar{\kappa}\bar{B}\bar{D} - \bar{y}\,\Gamma)^2\right]^2}. \tag{23b}$$

The profile of normalised shear stress is everywhere obtained from

$$\frac{\tau_{xy}}{\eta/\lambda} = -De_{\kappa}\left[\frac{\sinh(\bar{\kappa}\bar{y})}{\cosh(\bar{\kappa})} - \frac{\Gamma}{\bar{\kappa}}\bar{y}\right] \text{ or } \frac{\tau_{xy}}{-p_{,x}H/\Gamma} = \bar{\kappa}\frac{\sinh(\bar{\kappa}\bar{y})}{\cosh(\bar{\kappa})} - \Gamma\,\bar{y} \tag{24}$$

and that of the normalised first normal stress difference in layer II is given by

$$\frac{\tau_{xx}-\tau_{yy}}{\eta/\lambda} = 2De_{\kappa}^2\left[\frac{\sinh(\bar{\kappa}\bar{y})}{\cosh(\bar{\kappa})} - \frac{\Gamma}{\bar{\kappa}}\bar{y}\right]^2 \text{ or } \frac{\tau_{xx}-\tau_{yy}}{\left|-p_{,x}H/\Gamma\right|} = 2|De_{\kappa}|/\bar{\kappa}\left[\bar{\kappa}\frac{\sinh(\bar{\kappa}\bar{y})}{\cosh(\bar{\kappa})} - \Gamma\,\bar{y}\right]^2. \tag{25}$$

In layer I there is obviously no first normal stress difference. Note that the normalised shear stress must be independent of the fluid rheology, hence the second definition in Eq. 24 is preferred.

3.5 Nondimensional flow rate

Integration of the full nondimensional velocity profile gives the relationship between the flow rate per unit width, Q, and the independent variables, in particular the forcing parameter Γ, the viscosity ratio β, the EDL thickness $\bar{\kappa}$ and thickness ratio $\bar{\delta}_{\mathrm{L}}$. The normalized flow rate, which is defined as $\bar{Q} = Q/(u_{\mathrm{sh}}H)$ is given as the sum of the following five contributions

$$\bar{Q} = \bar{Q}_{\mathrm{E-I}} + \bar{Q}_{\mathrm{P-I}} + \bar{Q}_{\mathrm{E-II}} + \bar{Q}_{\mathrm{P-II}} + \bar{Q}_{\mathrm{EP-II}}, \tag{26}$$

which are expressed by:

$$\bar{Q}_{\mathrm{I}} = \bar{Q}_{\mathrm{E-I}} + \bar{Q}_{\mathrm{P-I}} = \beta\left\{\left[\bar{\delta}_{\mathrm{L}} + \frac{\bar{D}}{\bar{\kappa}}(\bar{F}-1)\right] - \frac{1}{6}\Gamma\bar{\delta}_{\mathrm{L}}^2\left(3-\bar{\delta}_{\mathrm{L}}\right)\right\} \tag{27a}$$

$$\bar{Q}_{\mathrm{E-II}} = \left(1-\bar{\delta}_{\mathrm{L}}\right)[\beta + \bar{E}(1-\beta)] - \frac{\bar{F}\bar{D}}{\bar{\kappa}} + \frac{2\varepsilon De_{\kappa}^2}{3}\left\{\left(1-\bar{\delta}_{\mathrm{L}}\right)\bar{E}\left(\bar{F}^2\bar{D}^2 - 2\bar{C}\right) - \frac{\bar{F}\bar{D}}{3\bar{\kappa}}\left(\bar{F}^2\bar{D}^2 - 6\bar{C}\right)\right\} \tag{27b}$$

$$\bar{Q}_{\mathrm{P-II}} = -\Gamma\left(1-\bar{\delta}_{\mathrm{L}}\right)\left\{2\left(1-\bar{\delta}_{\mathrm{L}}\right)^2\left[\frac{1}{6}+\frac{\varepsilon De_{\kappa}^2}{5\bar{\kappa}^2}\Gamma^2\left(1-\bar{\delta}_{\mathrm{L}}\right)^2\right]+\frac{1}{2}\beta\bar{\delta}_{\mathrm{L}}\left(2-\bar{\delta}_{\mathrm{L}}\right)\right\} \tag{27c}$$

$$\bar{Q}_{\mathrm{EP-II}} = \frac{\varepsilon De_{\kappa}^2\Gamma}{\bar{\kappa}^4}\left\{\bar{\kappa}^4\bar{C}\left(1-\bar{\delta}_{\mathrm{L}}\right)^3-\frac{3\bar{\kappa}\bar{E}\bar{F}\bar{D}}{2}\left[1+2\bar{\kappa}^2\left(1-\bar{\delta}_{\mathrm{L}}\right)^2\right]-\frac{3}{2}\bar{\kappa}^2\left(1-\bar{\delta}_{\mathrm{L}}\right)\left(\bar{C}-2\bar{E}^2\right)\right\} -\frac{6\varepsilon De_{\kappa}^2}{\bar{\kappa}^5}\Gamma^2\left[6\bar{F}\bar{D}-6\bar{\kappa}\bar{E}\left(1-\bar{\delta}_{\mathrm{L}}\right)+3\bar{\kappa}^2\bar{F}\bar{D}\left(1-\bar{\delta}_{\mathrm{L}}\right)^2-\bar{\kappa}^3\bar{E}\left(1-\bar{\delta}_{\mathrm{L}}\right)^3\right] \tag{27d}$$

4 Discussion of flow results

The above equations allow us to understand better the flow dynamics via some plots, which are analysed below. We start by looking at Fig. 3a, to pure EO flow ($\Gamma = 0$), which pertains to a situation with $\beta = 1$ and the corresponding normalised viscosity profiles in Fig. 4a. First, we focus on the analysis of the four Newtonian curves ($\varepsilon De_{\kappa}^2 = 0$) at different values of $\bar{\kappa}$ (curves with square symbols). Since $\beta = 1$ these four cases are indeed equivalent to a single Newtonian fluid. One of the effects we want to investigate in this work is that of the ratio between the thicknesses of the skimming layer and of the EDL, which is here carried out by fixing $\bar{\delta}_{\mathrm{L}}$ at 0.1 and varying $\bar{\kappa}$ (with $\bar{\delta}_{\mathrm{L}} \geq \bar{\kappa}^{-1}$ or $\bar{\delta}_{\mathrm{L}}\bar{\kappa} \geq 1$). These four profiles in Fig. 3a exhibit a large shear rate at the wall and a nearly constant plateau outside the EDL. Since the velocity is normalized by the Smoluchowski velocity and the viscosity is constant across the whole channel, the plateau value is equal to 1 and here the effect of EDL thickness is clear from the plot.

In reality, a skimming layer has usually a lower viscosity than the bulk fluid and this entails $\beta > 1$. Looking at the same four cases in Fig. 3b, i.e. the four curves pertaining to Newtonian fluid outside the skimming layer, this plot shows the corresponding velocity profiles for $\beta = 10$ all other quantities being identical. The corresponding viscosity profiles for $\beta = 10$ are plotted in Fig. 4b. Direct comparison between the Newtonian profiles in Fig. 3a, b shows that the normalised velocities with $\beta = 10$ are higher than those for $\beta = 1$ by a factor of up to 10. This does not correspond to higher dimensional velocities, but is rather a consequence of the use of the higher inner fluid viscosity coefficient (η) to calculate the Smoluchowski velocity scale used in the normalization. In fact, when the skimming layer is much thicker than the EDL, say $\bar{\kappa} = 100$ and $\bar{\delta}_{\mathrm{L}} = 0.1$, the fluid near the wall is still the same solvent of Fig. 3a and the electro-osmosis acts identically, but by using a velocity scale which is 10 times lower than the true Smoluchowksi velocity fictitiously increases the normalized velocity. We also observe that at the skimming layer interface the velocity profile is already constant, but as the thicknesses of the two layers approach each other the action of the EDL is felt directly inside as well as outside the skimming layer and at the interface the profile is no longer constant. In these cases the electro-osmosis effect reaches a lower maximum velocity and a kink is observed at the interface, because of the sudden increase in viscosity and the concomitant sudden reduction in shear rate associated with the constant value of the shear stress at the interface. Hence, values of $u/u_{\mathrm{sh}} < \beta$ indicate a reduction in the true flow rate due to the higher fluid viscosity outside the skimming layer. These findings are made clear if the data are replotted as Fig. 3c, where the same velocity profiles are now normalised with the Helmholtz–Smoluchowski velocity of the solvent, i.e. $u/u_{\mathrm{sh}}^{\mathrm{s}}$.

Still for pure EO flow the remaining curves (black lines) in Fig. 3a, b now analyse the effect of $\bar{\kappa}$ in combination with the effect of shear thinning quantified by parameter $\varepsilon De_{\kappa}^2$ for $\beta = 1$ and 10, respectively. The shear viscosity of an sPTT fluid is characterized by a Newtonian plateau at low shear rates followed by a shear-thinning behaviour that starts at a shear rate around $1/\lambda$ (cf. Eq. 6 and Fig. 2). Since in pure EO the high shear rates are found only near the wall, where the skimming layer is actually occupied by a Newtonian fluid, the fluid outside the skimming layer behaves essentially as a Newtonian fluid when $\bar{\delta}_{\mathrm{L}}\bar{\kappa} \gg 1$as is clear from the collapse of the curves for $\bar{\kappa} = 100$ and in spite of the large values of $\varepsilon De_{\kappa}^2$. This is also confirmed in the corresponding curves of Fig. 4, where the viscosity profiles for $\varepsilon De_{\kappa}^2 = 100$ and Newtonian fluids ($\varepsilon De_{\kappa}^2 = 0$) are coincident. As the thickness of the skimming layer approaches the thickness of the EDL ($\bar{\delta}_{\mathrm{L}}\bar{\kappa} \to 1$) then the shear thinning becomes noticeable because at the interface the shear rate is no longer negligible and a large variation in viscosity is seen (cf. Fig. 4).

Now, we must distinguish between the two situations shown in Fig. 3a, b. In Fig. 3b the situation is realistic with fluid outside the skimming layer being more viscous than the fluid inside the skimming layer ($\beta = 10$) and on crossing the interface from the skimming layer to the bulk fluid there is a sudden increase in flow resistance, a concomitant reduction in shear rate and an increase in viscosity. The shear-thinning effect is seen, but is rather limited and requires the EDL and the skimming layer thicknesses not to differ by too much. In fact, for $\bar{\kappa} = 100$ and at large values of $\varepsilon De_{\kappa}^2$, say $\varepsilon De_{\kappa}^2 = 100$, the profile of viscosity coincides with that for Newtonian fluids.

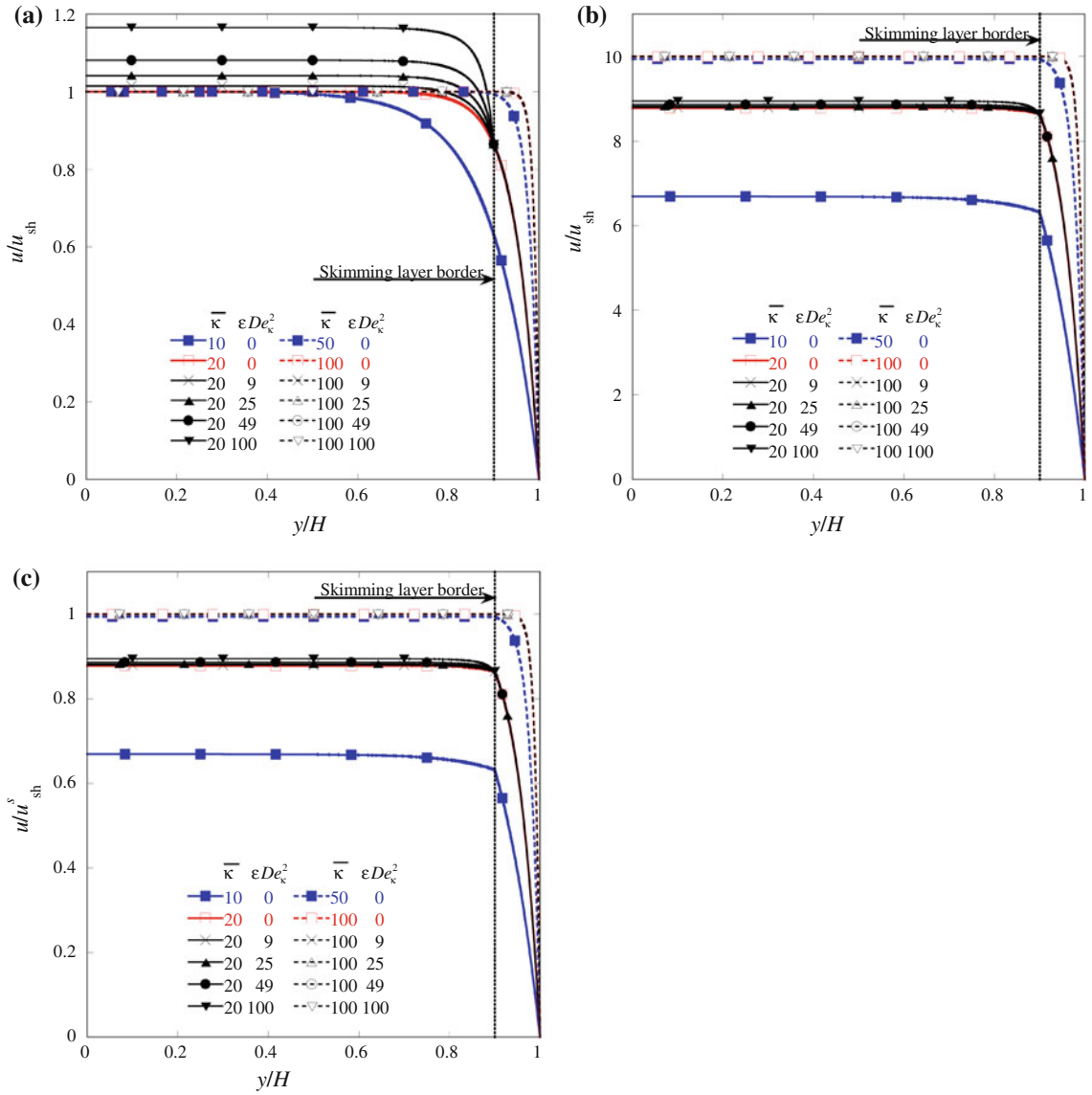

Fig. 3 Effects of $\bar{\kappa}$ and εDe_κ^2 on the profiles of normalized velocity for sPTT fluids in pure EO flow ($\Gamma = 0$) with $\bar{\delta}_L = 0.1$: **a** u/u_{sh} for $\beta = 1$, **b** u/u_{sh} for $\beta = 10$ and **c** u/u_{sh}^s for $\beta = 10$

In Fig. 3a there is apparently a large effect of εDe_κ^2, but the depicted situation is unrealistic since, with $\beta = 1$, the zero shear rate viscosity of the sPTT fluid is identical to the viscosity of the Newtonian fluid inside the skimming layer, meaning that at shear rates above the threshold of shear thinning the PTT fluid will be less viscous than the Newtonian fluid, as depicted in the corresponding viscosity plot of Fig. 4a. Here, we can also see that the sudden increase in the viscosity at the interface can even be as much as fivefold. This results in the observed large effect of shear thinning on the velocity profile for this particular limiting case, where in reality the bulk fluid will be more viscous than the skimming fluid corresponding to $\beta > 1$, i.e. the true situation is akin to that shown in Figs. 3b, c and 4b. In conclusion, for pure electroosmosis the effect of εDe_κ^2 is essentially non-existent when the EDL is much thinner than the skimming layer and fairly weak otherwise.

Figure 5 plots velocity profiles for Newtonian fluids in a situation with combined forcing (pressure gradient in addition to electro-osmosis). The plots in Fig. 5a correspond to a single fluid, since $\beta = 1$, and include both the adverse and favourable pressure gradients as well as the effect of $\bar{\kappa}$. The profiles are in agreement with those of Afonso et al. (2009) as they should. Except for the EDL region the normalized profiles are identical elsewhere for the same values of all other quantities but $\bar{\kappa}$, with the profiles at higher values of $\bar{\kappa}$ showing higher velocities near the wall. As these correspond to the single fluid of Afonso et al. (2009), the onset of reverse flow occurs for $\Gamma = 2$, even though this curve is not shown here. The

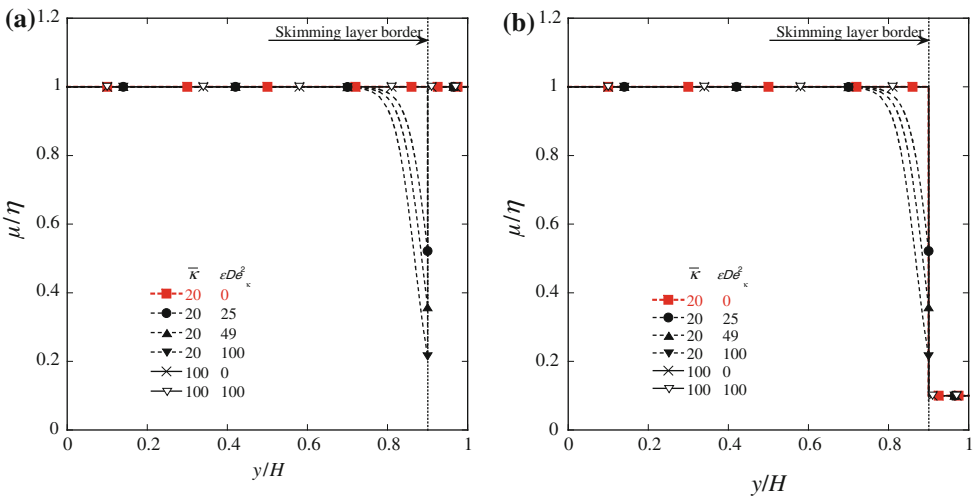

Fig. 4 Effects of $\bar{\kappa}$ and εDe_κ^2 on the profiles of normalized viscosity for Newtonian and sPTT fluids in pure EO flow ($\Gamma = 0$) with $\bar{\delta}_L = 0.1$: **a** $\beta = 1$ and **b** $\beta = 10$

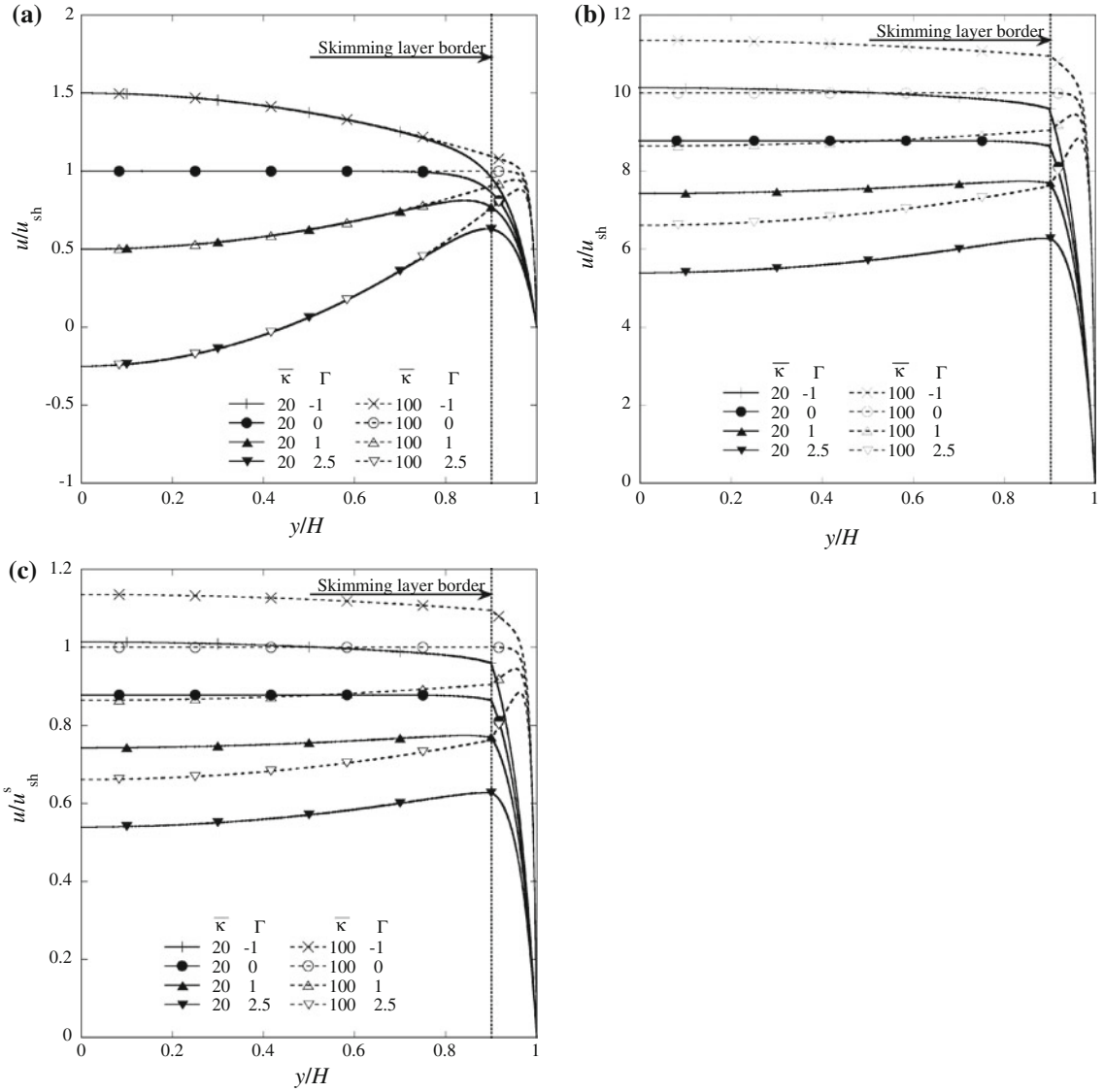

Fig. 5 Combined effect of $\bar{\kappa}$ and Γ on the profiles of normalized velocity of Newtonian fluids ($\varepsilon De_\kappa^2 = 0$) under combined forcing ($\Gamma \neq 0$) with $\bar{\delta}_L = 0.1$: **a** u/u_{sh} for $\beta = 1$, **b** u/u_{sh} for $\beta = 10$ and **c** u/u_{sh}^s for $\beta = 10$

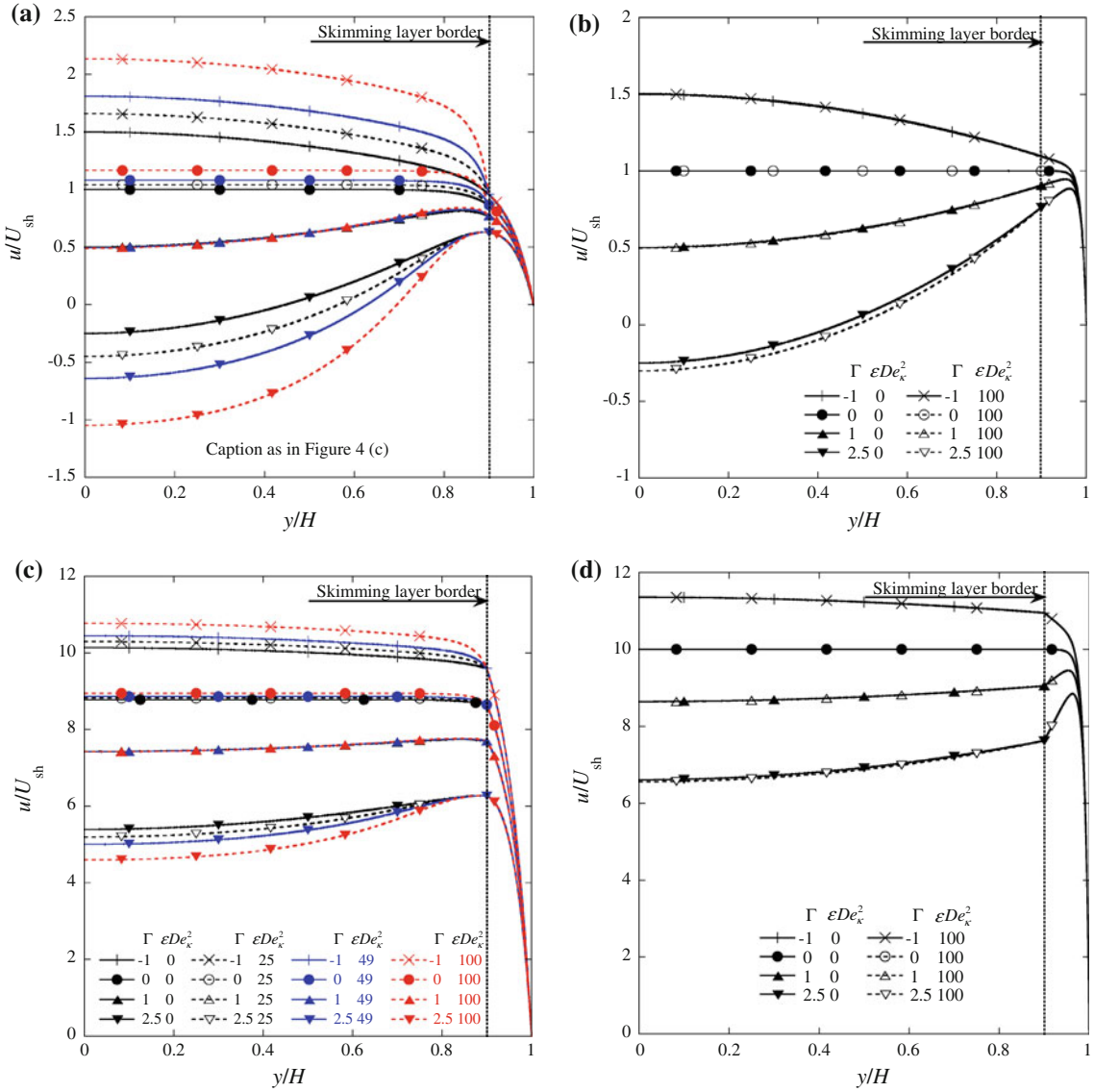

Fig. 6 Profiles of normalized velocity for sPTT fluids under combined forcing with $\bar{\delta}_L = 0.1$: **a** $\beta = 1$ and $\bar{\kappa} = 20$, **b** $\beta = 1$ and $\bar{\kappa} = 100$, **c** $\beta = 10$ and $\bar{\kappa} = 20$ and (d) $\beta = 10$ and $\bar{\kappa} = 100$

viscosity profiles corresponding to all cases in Fig. 5a are represented by a single thick line at constant $\mu/\eta = 1$ as in Fig. 4a.

When the bulk fluid is more viscous than the fluid in the skimming layer by a factor of 10 ($\beta = 10$), the corresponding velocity profiles are shown in Fig. 5b, all other parameters being equal, and the corresponding viscosity profile is represented by the thick line with a step in Fig. 4b (curve for $\varepsilon De_\kappa^2 = 0$). There are important qualitative differences between Fig. 5a and b. Velocity profiles for different values of $\bar{\kappa}$, with all other parameters identical, now are different. The value of Γ required for reverse flow is now larger and dependent of $\bar{\kappa}$. Since forcing is no longer exclusively by a surface mechanism the stresses are larger at the skimming layer interface than for pure EO flow and consequently the kink in the velocity profile is more apparent. Only part of the differences are related to the viscosity coefficient defining the Smoluchowski velocity scale used to normalise the profile. In fact, if the Newtonian solvent viscosity is used instead for normalisation, all the profiles are reduced by a factor of β, as is clear from the plots of u/u^s_{sh} of Fig. 5c, but their relative position remains the same as in Fig. 5b, so for $\Gamma = 2.5$ we still do not have reverse flow. Qualitatively the surface forcing mechanism acts exclusively on the low viscosity fluid (when $\bar{\delta}_L\bar{\kappa} \gg 1$), whereas the pressure forcing acts everywhere, i.e. for $\bar{\delta}_L = 0.1$ it acts upon the 81% of the total surface area occupied by the viscous fluid and on the 19% occupied by the Newtonian solvent, thus the pressure gradient needs to be stronger than in Fig. 5a in order to obtain the same profile.

Hence, it is clear that having a skimming layer with a less viscous fluid gives rise to different solutions than those for a single fluid.

Figure 6 shows plots for the sPTT fluid to investigate the combined effects of all parameters. When $\bar{\delta}_L\bar{\kappa} \gg 1$ ($\bar{\kappa} = 100$) and regardless of whether $\beta = 1$ or $\beta = 10$, the sPTT profiles are very close to the Newtonian profiles for εDe_κ^2 of up to 100. We observe shear-thinning effects for the cases with the largest adverse pressure gradient and a similar effect is expected for larger favourable pressure gradients than illustrated (not plotted for conciseness). However, these strong shear-thinning effects are only observed if simultaneously the value of εDe_κ^2 is quite large, because for low values of εDe_κ^2 and $|\Gamma|$ the range of shear rates outside the skimming layer are essentially within the first Newtonian plateau of the viscoelastic fluid. The viscosity profiles corresponding to some of the plots in Fig. 6 are shown in Fig. 7.

For small values of εDe_κ^2, a small shear-thinning effect is also observed when $\bar{\delta}_L\bar{\kappa} \to 1$ ($\bar{\kappa} = 20$) and especially for small values of β ($\beta = 1$), conditions which allow the shear rates outside the skimming layer to be in the power law region. As already mentioned, the conditions with $\beta = 1$ are unrealistic because the bulk fluid becomes less viscous than the skimming layer fluid (cf. Fig. 7a), but it is obvious that there is an intermediate range of conditions for which the shear-thinning characteristics of the fluid will have a non-negligible impact on the flow characteristics. This corresponds roughly to $1 < \beta < 10$ and $1 < \bar{\kappa}\bar{\delta}_L < 10$, but the upper limits of these two ranges may rise the larger the value of $|\Gamma|$.

The viscosity plots in Fig. 7a–c show the combined effects of εDe_κ^2, Γ, β and $\bar{\kappa}$. In all cases, the increase of εDe_κ^2 is to enhance the variation of μ/η with values of viscosity that near the interface can drop to values of the order of 10 of the zero shear viscosity in the bulk, even for the case with $\beta = 1$. If for this case the situation is unrealistic, because usually the fluid in the skimming layer is less viscous than outside, the trends in Fig. 7b are exactly the same for $\beta = 10$, which are physically sound. In this figure, it can also be observed under adverse pressure gradient flow conditions, the viscosity has a non-monotonic variation along the channel, exhibiting a local maximum and a local minimum. This is an interesting finding that corresponds to non-monotonic shear stress profiles, as

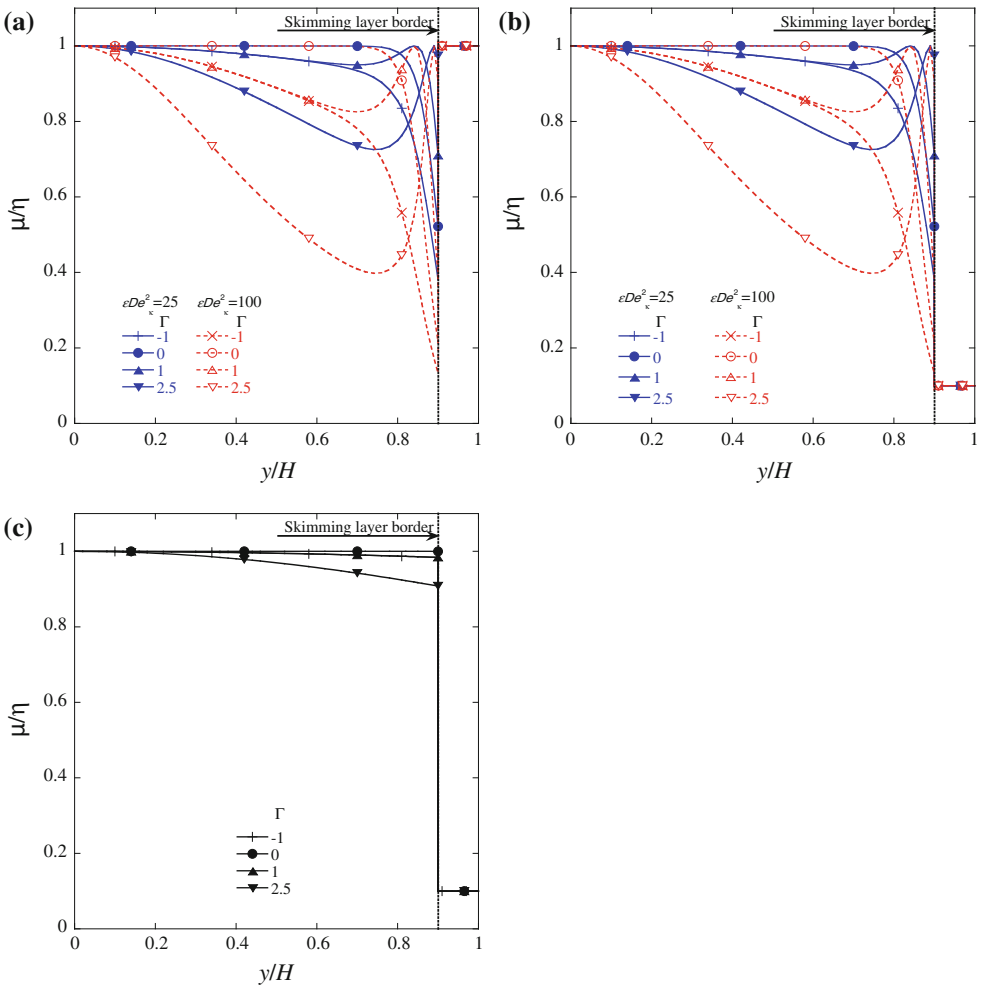

Fig. 7 Profiles of normalized viscosity for sPTT fluids under combined forcing with $\bar{\delta}_L = 0.1$: **a** $\beta = 1$ and $\bar{\kappa} = 20$, **b** $\beta = 10$ and $\bar{\kappa} = 20$, **c** $\beta = 10$, $\bar{\kappa} = 100$ and $\varepsilon De_\kappa^2 = 100$

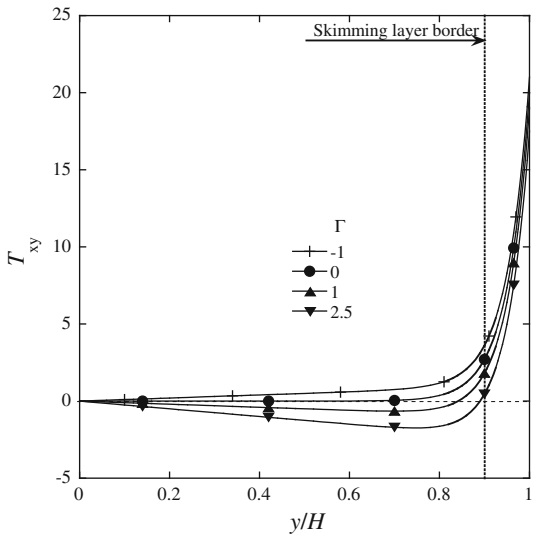

Fig. 8 Streamwise profiles of normalized shear stress under combined forcing for $\bar{\kappa} = 20$, $\bar{\delta}_L = 0.1$ and different values of Γ

shown in Fig. 8. Under conditions of very strong adverse pressure gradients, this originates a narrow near-wall region of fluid with multiple solutions, a situation that is prone to the occurence of flow instabilities.

For very thin EDLs ($\bar{\delta}_L\bar{\kappa} \gg 1$ such as for $\bar{\kappa} = 100$), the shear-thinning nature is negligible unless the pressure gradients are much larger in magnitude than shown in Fig. 7 (cf. Fig. 7c).

Figure 9 shows the variations of the total normalised flow rate, and of its components, with Γ and εDe_κ^2. For very thin EDL ($\bar{\kappa} = 100$) the dashed line of Fig. 9a indicates a negligible effect of εDe_κ^2, which is extensible to the range $-10 \leq \Gamma \leq 10$, a picture consistent with the velocity profiles. By reducing the value of $\bar{\kappa}$ to 20, the EDL and skimming layer thicknesses approach each other and we observe a non-negligible effect of εDe_κ^2 on the total flow rate both for favourable ($\Gamma < 0$) and adverse ($\Gamma > 0$) pressure gradients provided $|\Gamma| > 2$. Inspection of Fig. 9b, where the components of the total flow rate are plotted, provide insight into the way those effects occur. The plotted contributions are from pressure forcing ($\bar{Q}_P = \bar{Q}_{P-I} + \bar{Q}_{P-II}$), from electro-osmosis forcing ($\bar{Q}_E = \bar{Q}_{E-I} + \bar{Q}_{E-II}$) and the combined pressure gradient electro-osmosis ($\bar{Q}_{EP} = \bar{Q}_{EP-II}$) forcing.

By definition, there is no effect of Γ on $\bar{Q}_E$, and the effect of εDe_κ^2 is negligible. However, εDe_κ^2 has a non-negligible effect both upon $\bar{Q}_P$ and $\bar{Q}_{EP}$. Since Γ has a linear and a cubic contribution to $\bar{Q}_P$, it acts favourably or adversely according to its sign with the linear term dominating for $|\Gamma| \leq 3$ and the nonlinear taking over outside this range. The effect of εDe_κ^2 upon $\bar{Q}_P$ is combined with that of Γ^3, so that fluid elasticity becomes relevant also for $|\Gamma| > 3$. For a Newtonian fluid $\bar{Q}_{EP} = 0$ and Γ has both a linear and a quadratic contribution. However, inspection of Fig. 9b shows that Γ always acts favourably upon $\bar{Q}_{EP}$, thus indicating that the second non-linear term of Eq. 27d predominates over the first linear contribution.

5 Conclusions

Solutions of macromolecules tend to migrate towards or away from the walls depending on the interactive forces at play between the wall, the solvent and the molecules, thus forming either an adsorption or a skimming layer, respectively. When a layer depleted of molecules is formed, a possible model describing the behaviour of a viscoelastic fluid is that of skimming layer near the wall with a Newtonian fluid and an outer layer away from the wall with the unmodified viscoelastic solution. An analytical solution was derived for such a generalized model and the results have shown that the flow becomes dominated by the Newtonian wall layer especially when the EDL ($\bar{\kappa}^{-1}$) is much thinner than the skimming layer thickness ($\bar{\delta}_L$), even for large values of εDe_κ^2 and when the viscosity of the Newtonian fluid is much lower than the zero shear rate ($\beta \gg 1$).

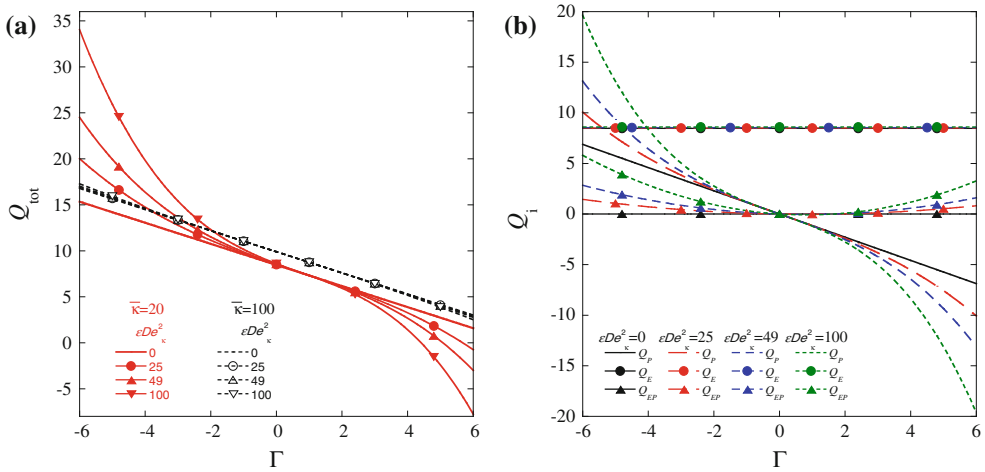

Fig. 9 Variation of normalized flow rates with Γ and εDe_κ^2 for $\beta = 10$ and $\bar{\delta}_L = 0.1$: **a** total flow rate as a function of $\bar{\kappa}$ and **b** Q_P, Q_E and Q_{EP} flow rate components

However, the shear-thinning nature of the viscoelastic fluid influences the flow characteristics at intermediate flow conditions, i.e. $1<\bar{\kappa}\bar{\delta}_{\mathrm{L}}<10$ and for $1<\beta<10$, so that under these conditions due account must be taken of the two layers of fluid.

One particular combination of forcings is that associated with the streaming potential for an imposed pressure gradient. Appendix derives the streaming potential for this flow of the PTT fluid with a Newtonian skimming layer, quantifying $E_{x\text{-sp}}$ and its corresponding nondimensional form, Γ_{sp}. The flow characteristics for this particular case are given by the same equations in the article provided $E_x = E_{x\text{-sp}}$ or $\Gamma = \Gamma_{\mathrm{sp}}$ and the above conclusions apply also.

Acknowledgements The authors wish to thank funding by Feder and Fundação para a Ciência e a Tecnologia (FCT) via project PTDC/EQU-FTT/70727/2006. A. M. Afonso also acknowledges FCT for financial support through scholarship SFRH/BD/28828/2006.

Appendix: Streaming potential

In the absence of an applied streamwise electric potential, the flow imposed by the pressure gradient creates a streaming current of ions $\left(I'_{\mathrm{s}}\right)$ which itself causes an electric potential (ϕ_{sp}) by the accumulation of counter-ions at the end of the channel. The gradient of this streaming potential is the streaming electrical field ($E_{x,\mathrm{sp}} = -\Delta\phi_{\mathrm{sp}}/l$), which is responsible for an opposite conduction current per unit width $\left(I'_{\mathrm{c}}\right)$ flowing both through the fluid and walls, depending on the total electric conductivity (σ_{t}). The equilibrium between the two currents defines the strength of the streaming potential. The conduction current is given by

$$I'_{\mathrm{c}} = 2\sigma_{\mathrm{t}}E_{x,\mathrm{sp}}H, \tag{28}$$

where $\sigma_{\mathrm{t}} = \sigma_{\mathrm{fluid}} + \sigma_{\mathrm{sur}}P_{\mathrm{sur}}/A_{\mathrm{chan}}$, with P_{sur} and A_{chan} denoting the wetted perimeter and cross-section area of the channel, respectively, and σ_{fluid} and σ_{sur} being the electric conductivities of the fluid and wall surface.

The streaming current per unit width is defined as

$$I'_{\mathrm{s}} = 2\int_0^H u(y)\rho_{\mathrm{e}}(y)\mathrm{d}y = 2u_{\mathrm{sh}}\left[\int_0^{H-\delta_{\mathrm{L}}} \bar{u}_{\mathrm{II}}(y)\rho_{\mathrm{e}}(y)\mathrm{d}y + \int_{H-\delta_{\mathrm{L}}}^{H} \bar{u}_{\mathrm{I}}(y)\rho_{\mathrm{e}}(y)\mathrm{d}y\right]. \tag{29}$$

Introducing a nondimensional parameter that quantifies the effect of electrical conductivity, $\Upsilon_1 = H^2\eta\sigma_{\mathrm{t}}/(\in^2\psi_0^2)$, the equilibrium steady state zero electric current condition $\left(I'_{\mathrm{c}} + I'_{\mathrm{s}} = 0\right)$ leads to the following cubic equation on $\Gamma_{\mathrm{sp}} \equiv -(H^2/(\in\psi_0))\left(p_{,x}/E_{x,\mathrm{sp}}\right)$

$$\Gamma_{\mathrm{sp}}^3 + a_1\Gamma_{\mathrm{sp}}^2 + a_2\Gamma_{\mathrm{sp}} + a_3 = 0. \tag{30}$$

with coefficients

$$a_1 = \frac{b'_2}{a'_2};\quad a_2 = \frac{c'_1 + c'_2}{a'_2} \quad \text{and} \quad a_3 = \frac{d'_1 + d'_2 - 2\Upsilon_1}{a'_2} \tag{31}$$

where

$$\begin{aligned}
c'_1 &= -\frac{\beta}{\bar{\kappa}}\left\{2(\bar{D}-\bar{\kappa}) + 2\bar{\kappa}\bar{E}\left(1-\bar{\delta}_{\mathrm{L}}\right) + \bar{F}\bar{D}\left[\bar{\kappa}^2\bar{\delta}_{\mathrm{L}}\left(2-\bar{\delta}_{\mathrm{L}}\right)-2\right]\right\}\\
d'_1 &= \beta\bar{\kappa}\left[\bar{\kappa}\bar{\delta}_{\mathrm{L}}\bar{C} - \bar{D} + \bar{F}\bar{D}(2-\bar{E})\right]\\
a'_2 &= \frac{4\varepsilon De_\kappa^2}{\bar{\kappa}^5}\left\{-3\bar{F}\bar{D}\left[2+\bar{\kappa}^2\left(1-\bar{\delta}_{\mathrm{L}}\right)^2\right] + \bar{E}\bar{\kappa}\left(1-\bar{\delta}_{\mathrm{L}}\right)\left[6+\bar{\kappa}^2\left(1-\bar{\delta}_{\mathrm{L}}\right)^2\right]\right\}\\
b'_2 &= \frac{\varepsilon De_\kappa^2}{\bar{\kappa}^3}\left\{\bar{\kappa}\left(1-\bar{\delta}_{\mathrm{L}}\right)\left[3\left(\bar{E}^2+\bar{F}^2\bar{D}^2\right)+2\bar{\kappa}^2\left(1-\bar{\delta}_{\mathrm{L}}\right)^2\bar{C}\right] - 3\bar{F}\bar{D}\bar{E}\left[2\bar{\kappa}^2\left(1-\bar{\delta}_{\mathrm{L}}\right)^2+1\right]\right\}\\
c'_2 &= \frac{1}{\bar{\kappa}}\left\{2\bar{\kappa}\overline{E}\left(1-\overline{\delta}_L\right) - \overline{F}\ \overline{D}\left[2-\beta\bar{\kappa}^2\overline{\delta}_L\left(2-\overline{\delta}_L\right)\right]\right\}\\
&\quad -\frac{\varepsilon De_\kappa^2}{12\bar{\kappa}}\left\{6\overline{E}\bar{\kappa}\left(1-\overline{\delta}_L\right)\left(\overline{E}^2+15\overline{C}+3\overline{F}^2\overline{D}^2\right)\right.\\
&\quad -\overline{F}\ \overline{D}\left(117\overline{C}+15\overline{E}^2+5\overline{F}^2\overline{D}^2\right)\\
&\quad +72\overline{F}\ \overline{D}\cosh\left(\bar{\kappa}\overline{\delta}_L\right)\sinh\left(\bar{\kappa}\overline{\delta}_L\right)\left[\bar{\kappa}\left(1-\overline{\delta}_L\right)\left(1+\overline{D}^2\right)-\overline{D}\right]\\
&\quad +36\overline{F}\ \overline{D}^2\sinh^2\left(\bar{\kappa}\overline{\delta}_L\right)\left[\overline{D}-2\bar{\kappa}\left(1-\overline{\delta}_L\right)\right]\\
&\quad \left.+36\overline{F}\ \overline{D}\cosh^2\left(\bar{\kappa}\overline{\delta}_L\right)\left[1-2\bar{\kappa}\overline{D}\left(1-\overline{\delta}_L\right)\right]\right\}\\
d'_2 &= \bar{\kappa}^2\left(1-\bar{\delta}_{\mathrm{L}}\right)\bar{C}\left(1-\frac{3}{2}\varepsilon De_\kappa^2\bar{C}\right)\\
&\quad +\frac{\varepsilon De_\kappa^2\bar{\kappa}}{6}\bar{E}\bar{F}\bar{D}\left(9\bar{F}^2\bar{D}^2-7\bar{E}^2\right)+\bar{\kappa}\bar{F}\bar{D}[2\beta(\bar{E}-1)-\bar{E}]\\
&\quad +\frac{4\varepsilon De_\kappa^2\bar{\kappa}\bar{F}\bar{D}}{3}\left\{\left[\bar{D}^3\sinh^3\left(\bar{\kappa}\bar{\delta}_{\mathrm{L}}\right)-\cosh^3\left(\bar{\kappa}\bar{\delta}_{\mathrm{L}}\right)\right]\right.\\
&\quad \left.+3\bar{E}\left[\bar{C}+\bar{D}\sinh\left(\bar{\kappa}\bar{\delta}_{\mathrm{L}}\right)\cosh\left(\bar{\kappa}\bar{\delta}_L\right)\right]\right\}
\end{aligned} \tag{32}$$

The solution of this cubic equation is given by

$$\Gamma_{\mathrm{sp}} = \sqrt[3]{-\frac{b_1}{2}+\sqrt{\frac{b_1^2}{4}+\frac{a^3}{27}}} + \sqrt[3]{-\frac{b_1}{2}-\sqrt{\frac{b_1^2}{4}+\frac{a^3}{27}}} - \frac{a_1}{3} \tag{33}$$

with coefficients a and b_1 as

$$a = a_2 - \frac{a_1^2}{3} \quad \text{and} \quad b_1 = a_3 - \frac{a_1a_2}{3} + \frac{2a_1^3}{27} \tag{34}$$

References

Afonso AM, Alves MA, Pinho FT (2009) Analytical solution of mixed electro-osmotic/pressure driven viscoelastic fluids in microchannels. J Non-Newton Fluid Mech 159:50–63

Alves MA, Pinho FT, Oliveira PJ (2001) Study of steady pipe and channel flows of a single-mode Phan-Thien–Tanner fluid. J Non-Newton Fluid Mech 101:55–76

Astarita G, Marrucci G (1974) Principles of non-Newtonian fluid mechanics. McGraw-Hill, Maidenhead

Berli CLA, Olivares ML (2008) Electrokinetic flow of non-Newtonian fluids in microchannels. J Colloid Interface Sci 320: 582–589

Bruus H (2008) Theoretical microfluidics, Oxford master series in condensed matter physics. Oxford University Press, Oxford

Burgreen D, Nakache FR (1964) Electrokinetic flow in ultrafine capillary slits. J Phys Chem 68:1084–1091

Chakraborty S (2007) Electroosmotically driven capillary transport of typical non-Newtonian biofluids in rectangular microchannels. Anal Chim Acta 605:175–184

Das S, Chakraborty S (2006) Analytical solutions for velocity, temperature and concentration distribution in electroosmotic microchannel flows in a non-Newtonian bio-fluid. Anal Chim Acta 559:15–24

Dutta P, Beskok A (2001) Analytical solution of combined electro-osmotic/pressure driven flows in two-dimensional straight channels: finite Debye layer effects. Anal Chem 73:1979–1986

Hunter RJ (2001) Foundations of colloid science. Oxford University Press, Oxford

Lyklema J, Rovillard S, De Coninck J (1998) Electrokinetics: the properties of the stagnant layer unravelled. Langmuir 14: 5659–5663

Olivares ML, Vera-Candiotti L, Berli CLA (2009) The EOF of polymer solutions. Electrophoresis 30:921–929

Oliveira PJ, Pinho FT (1999) Analytical solution for fully-developed channel and pipe flow of Phan-Thien–Tanner fluids. J Fluid Mech 387:271–280

Park HM, Lee WM (2008a) Helmholtz–Smoluchowski velocity for viscoelastic electroosmotic flows. J Colloid Interface Sci 317:631–636

Park HM, Lee WM (2008b) Effect of viscoelasticity on the flow pattern and the volumetric flow rate in electroosmotic flows through a microchannel. Lab-on-Chip 8:1163–1170

Park HM, Lee JS, Kim TW (2007) Comparison of the Nernst–Planck model and the Poisson–Boltzmann model for electroosmotic flows in microchannels. J Colloid Interface Sci 315:731–739

Phan-Thien N, Tanner RI (1977) New constitutive equation derived from network theory. J Non-Newton Fluid Mech 2:353–365

Probstein RF (2003) Physicochemical hydrodynamics, 2nd edn. Wiley Interscience, New Jersey

Reuss FF (1809) Sur un nouvel effet de l'électricité galvanique. Mémoires de la Societé Impériale des Naturalistes de Moscou 2:327–337

Vainshtein P, Gutfinger C (2002) On electroviscous effects in microchannels. J Micromech Microeng 12:252–256

Zhao C, Zholkovskij E, Masliyah JH, Yang C (2008) Analysis of electroosmotic flow of power-law fluids in a slit microchannel. J Colloid Interface Sci 326:503–510